PAPER

Classification of DC discharge modes based on acoustic signal

Physica Scripta

PAPER

Classification of DC discharge modes based on acoustic signal

RECEIVED
16 September 2022

REVISED
5 December 2022

ACCEPTED FOR PUBLICATION
14 December 2022

PUBLISHED
26 December 2022

Zilan Xiong*, Yuqi Wang and Mengqi Li

State Key Laboratory of Advanced Electromagnetic Engineering and Technology, Huazhong University of Science and Technology, Wuhan 430000, People's Republic of China

* Author to whom any correspondence should be addressed.

E-mail: zilanxiong@hust.edu.cn

Keywords: low temperature plasma, DC discharge, acoustic signal, discharge mode classification, support vector machine

Abstract

Gas discharge will produce rich electromagnetic, optical as well as acoustic signals. Compared with the other signals, acoustic signals are also significant and would offer non-contact, low cost and easy-operation approach for online discharging monitoring, which require more attention and intensive study. In this paper, we studied the characteristics of acoustic signals in the corona, transient glow, spark, and glow discharging modes generated in a DC pin-to-pin configuration and developed a method using acoustic signals to classify the different discharge modes. The acoustic signals of the discharge at different gaps were recorded by adjusting the gap distance. 250 sets of acoustic signal samples were collected for each discharging mode. It was found that acoustic signals behave differently in different modes. Based on the short-time Fourier transform (STFT) of the acoustic signals, a novel method for discharge mode classification using the support vector machine (SVM) approach was developed. The final predictive accuracy of the trained classifier exceeds 90%.

1. Introduction

Plasma produced by gas discharge has been widely used in many fields [1–4]. There are several device configurations for generating plasma in the atmosphere [5–9]. Compared with other plasma sources, the pin-pin configuration is simple and easy to control. Four typical discharge modes are usually observed in the pin-pin DC discharge, namely the corona, transient glow, spark, and glow modes [8, 10]. Owing to their different characteristics, plasmas in different modes have various applications. Corona discharge has prevalent industrial applications such as the electrostatic precipitator (ESP) for treatment of harmful gases [11]. Ozone generation is another common application of corona as an ion source, which can be used for disinfection of water supplies [12]. Because glow discharge operates in the steady-state regime, it is favorably applied in surface modification [13] and biomedical treatment [14]. Spark discharge is typically utilized in plasma ignition systems [15].

Under unsteady operating conditions, the discharging modes may transform from one to another. Therefore, distinguishing and monitoring the different types of discharge modes is a key issue in different applications. During discharge, electric, optical, electromagnetic, and acoustic signals are always produced [16–19]. The current methods used to classify discharge modes are usually based on these signal characteristics of plasma. The signal characteristics of plasma in different modes have distinct features and contain a large amount of information that can be used for mode classification. Compared with the traditional electromagnetic method, the acoustic method may provide a non-contact, low cost and easy operating approach for online discharging monitoring, therefore, the acoustic signal has become a popular classification method in recent years [19–24]. For example, based on the frequency domain characteristics of acoustic signals, artificial neural networks can be built to distinguish partial discharges in outdoor insulation systems, which is essential to the safety of equipment [23, 24]. This approach has the advantages of fast response, low cost, and non-contact, which are important for industrial application. Compared to other signals in plasma, the characteristics of acoustic signals in different discharging modes still lack a systematic study, and the use of acoustic signals for mode classification requires further development.

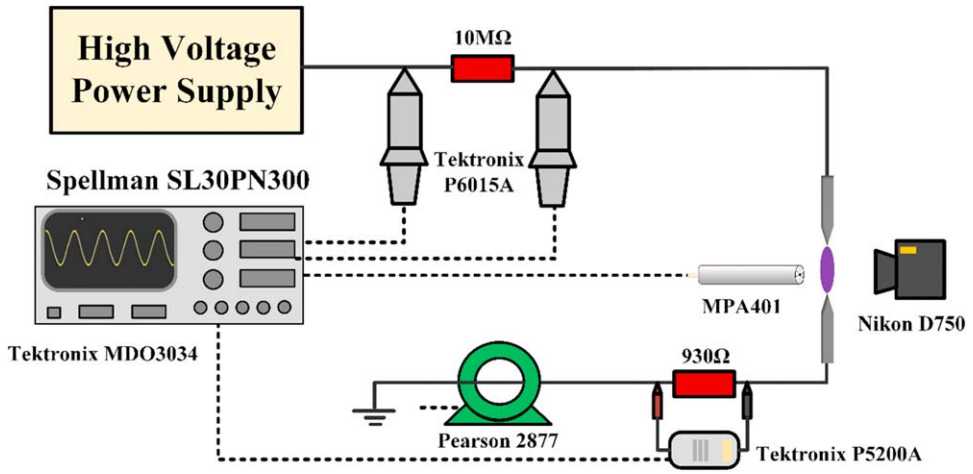

Figure 1. Experimental setup.

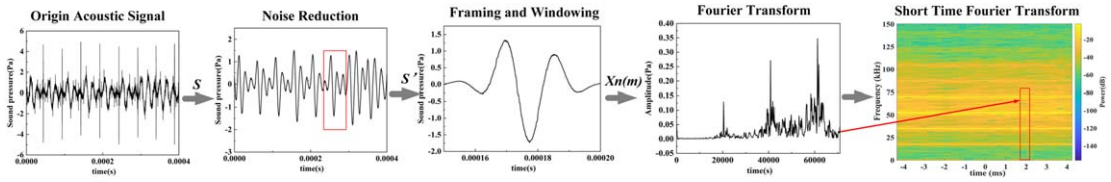

Figure 2. Process of STFT feature extraction.

In this study, the acoustic signals of different DC discharge modes were measured and analyzed. The short-time Fourier transform (STFT) of each mode was then extracted. Based on this feature, the support vector machine (SVM) approach was proposed to train the classifier to identify discharge modes.

2. Experimental setup and methods

2.1. Experimental setup

Figure 1 illustrates the schematic of the experimental setup. Two stainless needles were used as electrodes to generate plasma driven by a DC power supply (Spellman SL30PN300) and were fixed on the slide rail. The gap between the two needle tips was adjusted to obtain different discharge modes. A ballast resistor (R = 10 MΩ) was connected in series in the circuit. For all the experiments, the applied voltage was fixed at 14 kV. The data of all signals were acquired simultaneously using an oscilloscope (Tektronix MDO3034). The applied and discharge voltages were monitored using voltage probes (Tektronix P6015A). A current probe (Pearson 2877) was used to measure the pulsed current. The voltage V_r across the small resistor (r = 930 Ω) was measured using a differential probe (Tektronix P5200A). Subsequently, the direct current in the circuit was calculated according to $I = V_r/\mathrm{r}$. A microphone (BSWA MPA401) was used to record the acoustic signal generated by the plasma. It was situated at the same altitude as the discharge region but 10 cm away. The images during discharge were captured by a digital camera (NIKON D750) with an exposure time of 0.4 s.

2.2. Methods of feature extraction

The extraction of suitable features is an important issue in the classification of discharge modes. Generally, to fully characterize the acoustic signal, the time-frequency diagram calculated by STFT [25, 26] is used to analyze how the frequency content of a nonstationary signal changes over time. Figure 2 shows the basic steps of signal processing.

Burrs and electromagnetic interference commonly exist in the waveform of the collected acoustic signal; therefore, noise reduction is necessary before feature extraction. A median filter is widely applied to remove glitches from waveform. The basic principle is to replace the value of each point in the signal to be processed with the median value of all points in its neighborhood. First, a sliding window of odd length is specified to move over the signal to be filtered, sample by sample. Then the data in the window is sorted by size, and the median is taken

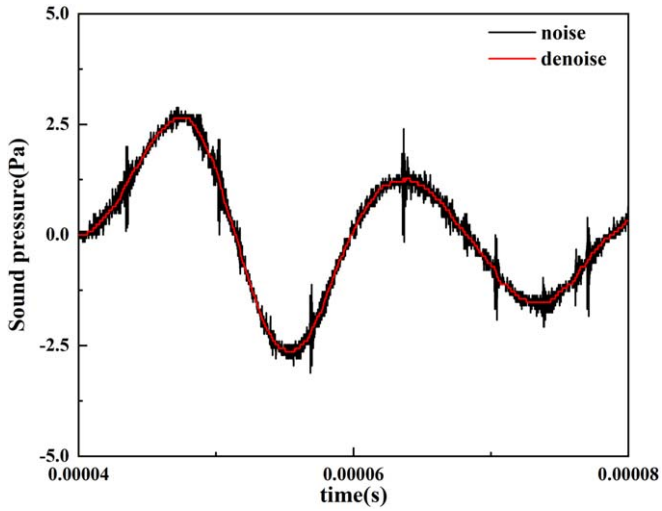

Figure 3. Denoising result of acoustic signal.

as the new data in the middle point of the original window. Samples of the denoising results are presented in figure 3. This approach eliminates isolated noise points without destroying signal characteristics.

Since the acoustic signal is not stationary, it is commonly segmented into frames of the same length; the signal is considered to be fairly stable within each frame. To avoid loss of dynamic information, the overlapped frames are usually specified, which compensates for signal attenuation at the edges. In addition, to reduce spectral ringing, each frame is often multiplied by a Hamming window function, which tapers off at the edges. Subsequently, the nth frame of the signal obtained after framing and windowing is $x_n(m)$, which is defined as

$$x_n(m) = w(m)x(n + m)0 \leqslant m \leqslant N - 1, \tag{1}$$

where $w(m)$ is the window function, N is the frame length, n is the frame number, and m is the time sequence of frame synchronization.

The Fourier transform (FT) was then performed on each windowed frame, and the calculation results were added to the STFT matrix that contained the magnitude and phase for each point in time and frequency. The mth element of this STFT matrix is

$$X_n(k) = \sum_{m=0}^{N-1} x_n(m)\mathrm{e}^{-j\frac{2\pi km}{N}}0 \leqslant k \leqslant N - 1, \tag{2}$$

where $X_n(k)$ represents the amplitude estimation of $x(n)$. The power $P_n(k)$ of the acoustic signal was estimated by determining the square norm of the amplitude spectrum as follows:

$$P_n(k) = 10 \times \log_{10}\left(|X_n(k)|^2 \times \frac{1}{N}\right) \tag{3}$$

2.3. Principle and application of SVM

Currently, there are many classification methods, such as k-nearest neighbor (k-NN), artificial neural network (ANN), and support vector machine (SVM). Among these, SVM is a simple method for solving classification problems involving few samples and nonlinear high-dimensional conditions, and is thus suitable for this study.

SVM is mainly intended for binary classification, and its basic principle is to construct the separating hyperplane with the largest margin between the two classes [27]. Based on this principle, SVM can be expanded to solve multiclass problems via a one-against-one strategy [28]. This strategy constructs SVM models between every pair of classes to form a parallel architecture. For the training data from the ith and jth classes, SVM solves via the following formulation [29, 30].

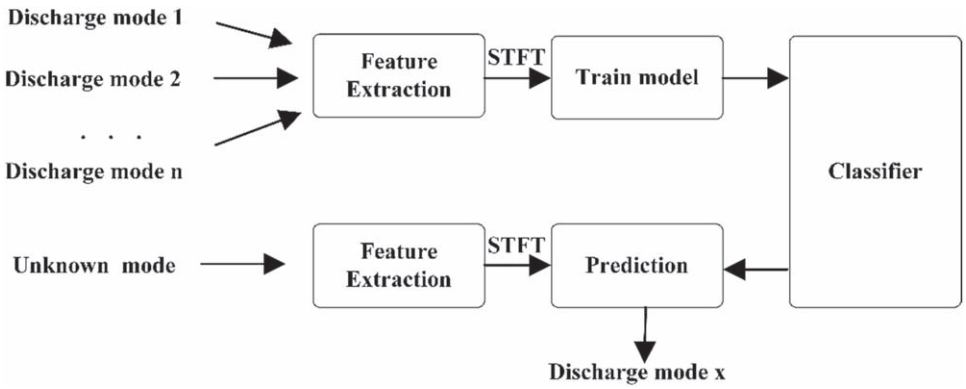

Figure 4. Diagram of SVM framework.

$$\begin{aligned} &\min_{\omega^{ij},b^{ij},\xi^{ij}} \frac{1}{2}(\omega^{ij})^T\omega^{ij} + C\sum_t \xi_t^{ij}(\omega^{ij})^T \\ &s.t.\ (\omega^{ij})^T\phi(x_t) + b^{ij} \geqslant 1 - \xi_t^{ij},\ if\ y_t = i \\ &(\omega^{ij})^T\phi(x_t) + b^{ij} \leqslant -1 + \xi_t^{ij},\ if\ y_t = j \\ &\xi_t^{ij} \geqslant 0 \end{aligned} \tag{4}$$

The decision function of SVM between the ith and the jth classes is

$$y_{\text{new}}^{ij} = \text{sign}[\ (\omega^{ij})^T\phi(x_{\text{new}}) + b^{ij}]. \tag{5}$$

For new data, the voting strategy is used for classification; if predicted to belong to the ith class by the decision function, a favorable vote is added for the ith class. Otherwise, the jth-class votes are increased by one. Then according to the votes for two classes, the final decision is taken based on the 'Max Wins' rule.

A diagram demonstrating the SVM approach used in this study for the classification of DC discharge modes is shown in figure 4. First, the acoustic signals in different discharge modes are collected. Next, the features that distinguish members of different signal classes are extracted as the input to train the SVM classifier. For the acoustic signals of the unknown modes, the predicted classification of the discharge modes can be obtained as long as the extracted features are input into the pre-trained classifier.

3. Results and discussion

3.1. Features and measurement in discharge modes

In order to achieve accurate classification, the characteristics of different discharge modes were recorded and analyzed in detail. As shown in figure 5, the powered electrode was on the upper side, whereas the grounded electrode was on the opposite side. Based on existing research, in this study, different discharging modes were categorized according to their appearance during discharge [8, 10]. Four discharge modes could be clearly observed by adjusting the discharge gap. The electric and acoustic signals of different modes were measured, and the characteristics of the plasma sound in the time-frequency domain were analyzed.

The time, frequency, and intensity are the three significant characteristics of acoustic signal. However, neither the time domain nor the frequency domain characteristics can completely describe the change of acoustic signal, then a time-frequency diagram of STFT is commonly used to solve this problem. Three characteristics can be displayed in the 2D plot, realizing the visualization of acoustic signal. This diagram takes time as the abscissa and frequency as the ordinate and the points with color represent the power of the acoustic signal.

Corona discharge appeared at 17–20 mm, and the discharge frequency ranged between 80 and 130 kHz. As shown in figure 5(a), at 20 mm, there is weak plasma around the two needle tips; the air gap does not break down completely. In each discharge cycle, the peak value of current pulse is about 1.5 mA and the drop voltage is approximately 10 V. No obvious audible sound could be heard in the actual experiment because the amplitude of the acoustic signal was small—mainly between −0.04 and 0.04 Pa. With regard to the time-frequency domain, the corona generally operated in a steady state, with no sudden change during 10 ms. The component of the spectrum in the corona mode was mainly below 50 kHz, of which the acoustic signal had a characteristic spectrum with approximately 46 kHz and −42 dB, which was beyond the auditory response range of the human ear.

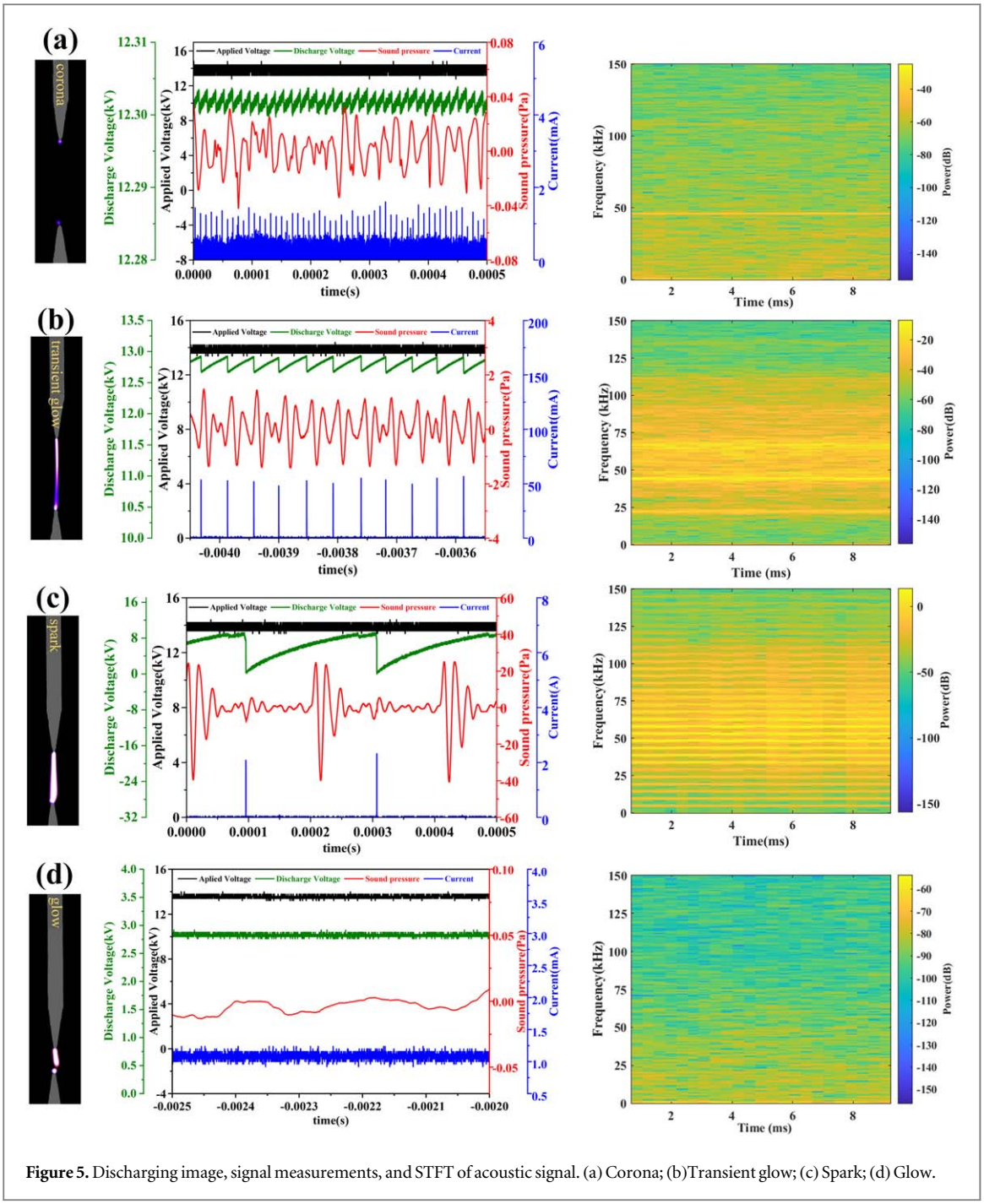

Figure 5. Discharging image, signal measurements, and STFT of acoustic signal. (a) Corona; (b)Transient glow; (c) Spark; (d) Glow.

The discharge mode changed to transient glow discharge when the distance was reduced to approximately 13–16 mm, and the repetition frequency of the discharge ranged between 13 and 20 kHz. An image of the transient glow discharge is presented in figure 5(b). It can be seen that there is a bright plasma column, a brief dark region, and a small bright area in that order from anode to cathode. The drop voltage increases to approximately 300 V and the peak value of current increases to approximately 60 mA. Meanwhile, during discharge, a weak sibilant sound could be heard clearly. The time-domain waveform of the acoustic signal is composed of a series of random sound pressure pulses with bipolar properties, and the amplitude is not large. Here, the collected signal at 15 mm is taken as an example, in which the first positive amplitude P_m is approximately 1.12 Pa whereas the first negative amplitude N_m is approximately −1.28 Pa. From the STFT graph, three distinct frequency bands can be observed: approximately, 20 kHz, 44 kHz, and 66 kHz. It should be noted that the spectral components in the audible range have amplitude of approximately −20 dB, which is lower than that of other high-frequency components, and the value of the power spectrum around 44 kHz is the greatest, at approximately −14 dB.

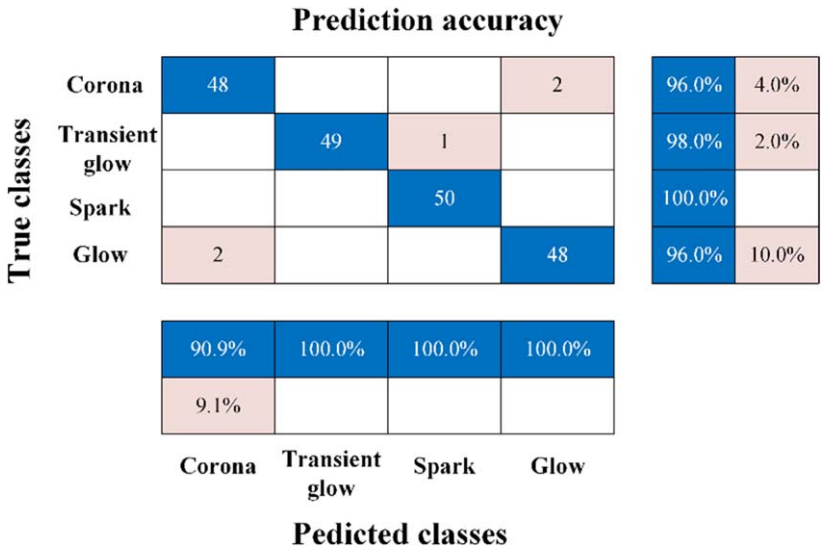

Figure 6. The confusion matrix of prediction results.

As the discharge distance decreased to 7–11 mm, spark discharge occurred, and the discharge frequency was approximately 4–9 kHz. As shown in figure 5(c), the air gap is completely broken down, accompanied by intense white-light emission and a loud buzzling sound. The peak-to-peak value of discharge voltage is relatively high, approximately 9 kV, and the peak value of current increases to approximately 2.1 A. The waveform of the acoustic signal is also a bipolar pulse, but the amplitude of the sound pressure is much larger than that in other modes. The measurement shown in figure 5(c) is obtained at 11 mm, in which the first positive amplitude P_m of the acoustic signal is approximately 24.6 Pa and the first negative amplitude N_m is approximately −39.8 Pa. As displayed in the STFT graph, more frequency bands can be observed, containing approximately 6 kHz and multiples of basic frequency. Furthermore, the power spectrum of the frequency components within the auditory response range of humans is approximately −12.8 dB, which is much lower than that of the components outside the audible range, approximately 13.5 dB.

Finally, the final mode was glow discharge, which occurred at less than 6 mm, and was DC discharge. As shown in the image of 5 mm in figure 5(d), it is evident that the regime includes a positive column, Faraday dark space, and negative glow. In this mode, the discharge current and voltage are both in the DC state, where the voltage is approximately 2.8 kV and the current is approximately 1.2 mA. The amplitude of the filtered acoustic signal had almost no fluctuation, which means that no sound waves could be measured. In fact, no sound was heard during glow discharge in the experiment. The STFT graph also shows that the spectrum mainly consists of a DC component, and its intensity is approximately −58 dB.

It should be noted that there exists the phase mismatch between electric and acoustic signal, especially obvious in transient glow and spark modes. There is about 320 μs time delay between the sound pulse and the current pulse, which is mainly determined by the measuring distance. The speed of sound under atmospheric pressure is about 340 m s^{-1}, and in our experiment, the microphone was ~10 cm away from the discharge gap, which may cause ~300 μs time delay. Simultaneously, considering the factors such as the propagation delay of the signal cable, these would both lead to the phase mismatch of signal in time domain.

From the above results, it might be inferred that the generation of acoustic signal is related to electric signal. The air gap is broken down owing to the injection of discharge energy. Hence, a large amount of heat is produced in a short time via electron-impact and dissociative quenching reactions [31, 32]. This leads to hydrodynamic expansion of the air, and then sound wave is generated during the gas discharge process.

3.2. Classification of discharging modes

According to the STFT features discussed above, the SVM approach was proposed for classification of different discharge modes. The acoustic signals of the discharge at different gaps were collected by adjusting the discharge distance. In this study, 250 sets of acoustic signal samples were collected for each mode, of which 80% were used for training the SVM classifier and the remaining 20% were used to verify the prediction accuracy of the trained classifier. The training accuracy of the SVM classification method based on the STFT features of the acoustic signal reached up to 92.6%. Simultaneously, the final results of the validation were analyzed using a confusion matrix, where the rows of the confusion matrix represented the true classes whereas the columns represented the predicted classes. As shown in figure 6, one of the spark modes is mistakenly classified as a transient glow mode,

Table 1. Prediction accuracy of three tests.

Number of times	1	2	3
Prediction accuracy	92.5%	97.5%	90%

two corona modes are mistakenly classified as glow, and two glow modes are mistakenly classified as corona. The prediction accuracy of the classifier for the four modes was as follows: 96% for corona, 98% for transient glow, 100% for spark, and 96% for glow. The overall prediction accuracy of the classifier was as high as 97.5%.

To ensure the stability of the classification model, acoustic signal samples without predicted labels were used for the test. Eighty sets of data were input into the trained classifier each time, that is, 20 samples for each mode. The test was repeated thrice, and the results are presented in table 1. The prediction accuracy of all the tests exceeded 90%, which proves that the classification method was effective.

Gas discharge in air under atmospheric pressure is affected by many factors, such as the temperature, the ambient humidity, the air impurity and so on [33, 34]. These factors will also the propagation characteristic of the acoustic wave [35, 36]. In this primary study, we aimed at investigating the characteristics of acoustic signal in different discharge modes, and developing a new method for modes classification based on acoustic signals. How these factors that will affect the discharge modes and the characteristics of acoustic signal will be further investigated in our following work. However, it's obvious that the acoustic signals of different discharge modes have different characteristics and can be taken as the feature for mode classification.

4. Conclusion

In this study, the acoustic signal characteristics of four DC discharging modes generated in a pin-to-pin configuration were presented. Moreover, based on the time-frequency domain feature STFT of each mode, an SVM method was proposed to train the classifier to identify discharge modes. The final predictive accuracy of the trained classifier exceeds 90%. Accordingly, the acoustic signal of discharge could be an effective method for mode classification. Future works will focus on the investigating the influential factors on the characteristics of acoustic signal in different discharge modes and utilizing other features of acoustic signals or classifiers to improve classification accuracy according to different discharge configurations.

Acknowledgments

This work is supported by National Natural Science Foundation of China (No. 52177145).

Data availability statement

All data that support the findings of this study are included within the article (and any supplementary files).

ORCID iDs

Zilan Xiong https://orcid.org/0000-0003-1095-3959

References

[1] Zhu Y, Xiong Z, Li M, Chen X, Lu C and Zou Z 2021 Investigation of NH_4NO_3 formation by air plasma and wasted ammonia *Plasma Process. Polym.* **18** 1–7
[2] Huang Y H and Wang M J 2020 Atmospheric pressure plasma jet-assisted copolymerization of sulfobetaine methacrylate and acrylic acid *Plasma Process. Polym.* **17 e 1900209**
[3] El-Naggar H I, Al-Halim M A A, Gaballa A S and Hassouba M A 2021 Surface improvement of cotton/polyester blend textile using DC air glow discharge plasma *Phys. Scr.* **96** 125712
[4] Rathore V and Nema S K 2022 The role of different plasma forming gases on chemical species formed in plasma activated water (PAW) and their effect on its properties *Phys. Scr.* **97** 065003
[5] Boudjadar A, Bouanaka F and Rebiaï S 2022 Physical phenomena of a cold plasma jet model at atmospheric pressure *Phys. Scr.* **97** 125609
[6] Sun Y, Liu X, Dong K and Xie C 2019 Corona discharge effect on charge and energy transfer in dielectric barrier discharge *Phys. Scr.* **94** 085602
[7] Zou Z, Han R, Lu C and Xiong Z 2021 Detection of long-lived species in plasma-activated water, based on digital colorimetry *Plasma Process. Polym.* **18** 1–12

[8] Wu S, Cheng W, Huang G, Wu F, Liu C, Liu X, Zhang C and Lu X 2018 Positive streamer corona, single filament, transient glow, dc glow, spark, and their transitions in atmospheric air *Phys. Plasmas* **25** 123507
[9] Fan R, Wang Y, Zhang X, Tu Z and Zhang J 2021 The regulation of memory effect and its influence on discharge properties of a dielectric barrier discharge driven by bipolar pulse at atmospheric-pressure nitrogen *Plasma Sci. Technol.* **23** 105401
[10] Machala Z, Jedlovský I and Martĭsovitš V 2008 DC discharges in atmospheric air and their transitions *IEEE Trans. Plasma Sci.* **36** 918–9
[11] Napartovich A P 2001 Overview of atmospheric pressure discharges producing nonthermal plasma *Plasmas Polym.* **6** 1–14
[12] Wattieaux G, Ferrer V, Sarrette J-P, Merbahi N and Eichwald O 2022 Experimental mapping of the ozone distribution in a pulsed positive corona discharge to estimate the efficiency of ozone production *Phys. Scr.* **97** 125608
[13] Moritz S, Moritz S, Schmidt A, Schmidt A, Sann J, Sann J, Thoma M H and Thoma M H 2020 Surface modifications caused by cold atmospheric plasma sterilization treatment *J. Phys. D: Appl. Phys.* **53** 325203
[14] Shimizu T 2020 Wound treatment by low-temperature atmospheric plasmas and issues in plasma engineering for plasma medicine *Jpn. J. Appl. Phys.* **59** 120501
[15] Nakamura T, Takahashi E, Nishioka M and Teraji T 2021 Long gap spark discharge ignition using a boron-doped diamond electrode *J. Phys. D: Appl. Phys.* **54** 405204
[16] Janda M, Machala Z, Dvonč L, Lacoste D and Laux C O 2015 Self-pulsing discharges in pre-heated air at atmospheric pressure *J. Phys. D: Appl. Phys.* **48** 035201
[17] Zhang Y, Qin Y, Zhao G and Ouyang J 2016 Time-resolved analysis and optical diagnostics of Trichel corona in atmospheric air *J. Phys. D: Appl. Phys.* **49** 0–10
[18] Liu W, Zheng Q, Hu M, Zhao L and Li Z 2019 Study of generation characteristics of glow- type atmospheric-pressure plasma jet based on DC discharge in air *Plasma Sci. Technol.* **21** 125404
[19] Algeelani N A and Piah M A M 2011 Identification of acoustic signals of surface discharges on glass insulator under different contamination levels *InECCE 2011 - Int. Conf. Electr. Control Comput. Eng.* pp 511–4
[20] Chai M L, Md Thayoob Y H, Ghosh P S, Sha'ameri A Z and Talib M A 2006 Identification of different types of partial discharge sources from acoustic emission signals in the time-frequency representation *First Int. Power Energy Conf. (PECon 2006) Proc.* pp 581–6
[21] Zou H, Chen H, Liu Z and Wang G 2021 Research on power equipment fault diagnosis technology based on acoustic signal research on power equipment fault diagnosis technology based on acoustic signal *IOP Conf. Series Earth and Environmental Science* vol 769042099
[22] Accounting F, Chen Y and Xu D 2022 Study on partial discharge fault diagnosis of high voltage switchboard based on ultrasound detection *J. Phys. Conf. Ser.* **2260** 012030
[23] Polisetty S, El-Hag A and Jayram S 2019 Classification of common discharges in outdoor insulation using acoustic signals and artificial neural network *High Volt.* **4** 333–8
[24] Harbaji M, Shaban K and El-Hag A 2015 Classification of common partial discharge types in oil-paper insulation system using acoustic signals *IEEE Trans. Dielectr. Electr. Insul.* **22** 1674–83
[25] Wei W, Liang C, Yang Z, Xu P, Yan X, Gao G and Wu G 2019 A novel method for detecting the pantograph–catenary arc based on the arc sound characteristics *Proc. Inst. Mech. Eng. Part F J. Rail Rapid Transit* **233** 506–15
[26] Gao Z B 2012 Short time fourier transform analysis of multi-component nonstationary acoustic signal *Adv. Mater. Res.* **403–408** 3163–5
[27] Hsu C W and Lin C J 2002 A comparison of methods for multiclass support vector machines *IEEE Trans. Neural Networks* **13** 415–25
[28] Gualtieri J 1999 Support vector machines for hyperspectral remote sensing classification *Proc. SPIE- Int. Soc.* **1** 1–12
[29] Vapnik V N 2000 The Nature of Statistical Learning Theory (New York: Springer) 2nd edn (https://doi.org/10.1007/978-1-4757-3264-1)
[30] Melgani F and Bruzzone L 2004 Classification of hyperspectral remote sensing images with support vector machines *IEEE Trans. Geosci. Remote Sens.* **42** 1778–90
[31] Popov N A 2013 Fast gas heating initiated by pulsed nanosecond discharge in atmospheric pressure air *51st AIAA Aerosp. Sci. Meet. Incl. New Horizons Forum Aerosp. Expo.* **2013** 1–20
[32] Popov N A 2001 Investigation of the mechanism for rapid heating of nitrogen and air in gas discharges *Plasma Phys. Reports* **27** 886–96
[33] Chen S, Li K, Wang F, Sun Q and Zhong L 2019 Effect of humidity and air pressure on the discharge modes transition characteristics of negative DC corona *IET Sci. Meas. Technol.* **13** 1212–8
[34] Xi W, Luo S, Liu D, Wang Z, Liu Z, Guo L, Wang X and Rong M 2022 The effect of humidity on the discharge mode transition of air discharge plasma *Phys. Plasmas* **29** 090701
[35] Program N M and Africa S 1993The variation of the specific heat ratio and the speed of sound in air with temperature, pressure, humidity, and CO_2 concentration *J. Acoust. Soc. Am.* **93** 2510–6
[36] Yi Y, Chen Z and Wang L 2016 Influence of humidity on spectrum characteristics of audible noise of DC transmission lines *Annu. Rep. - Conf. Electr. Insul. Dielectr. Phenomena, CEIDP* **2016** 275–8